Catena 133 (2015) 441–451

Contents lists available at ScienceDirect

Catena

journal homepage: www.elsevier.com/locate/catena

Relative sea-level and climatic changes in the Amazon littoral during the last 500 years

Marcelo Cancela Lisboa Cohen [a,b,*], Igor Charles Castor Alves [a,b], Marlon Carlos França [a], Luiz Carlos Ruiz Pessenda [c], Dilce de Fátima Rossetti [d]

[a] Laboratory of Coastal Dynamics, Graduate Program of Geology and Geochemistry, Institute of Geoscience, Federal University of Pará (UFPA), Rua Augusto Correa 01, 66075-110 Belém, PA, Brazil
[b] Faculty of Oceanography, Federal University of Pará, Rua Augusto Corrêa, n 1, Guama, CEP: 66075-110 Belém, PA, Brazil
[c] Center for Nuclear Energy in Agriculture (CENA), 13400-000 Piracicaba, SP, Brazil
[d] National Institute for Space Research (INPE), Rua dos Astronautas 1758-CP 515, CEP: 12245-970 São José dos Campos, SP, Brazil

ARTICLE INFO

Article history:
Received 6 March 2015
Received in revised form 27 May 2015
Accepted 18 June 2015
Available online xxxx

Keywords:
Amazonia
Mangrove
Organic matter sources
Palynology
Sedimentary facies

ABSTRACT

An integrated approach focused on sedimentology, geochemistry, palynology, C and N isotopes and radiocarbon dating of a sediment core from an herbaceous plain not flooded by tides of the Amapá littoral, near the Amazon River mouth, allowed identification of two phases with marine and terrestrial influences. Mangroves occurred over tidal mud flats with marine influence between >5610–5470 and 470–310 cal yr BP. The absence of mangrove vegetation since 470–310 cal yr was followed by the transition of brackish water organic matter to terrestrial C_3 plants. Also, the geochemical data indicate a decrease in sea water influence during this last time interval. Likely, the displacement of mangrove forest to lower surfaces was caused by a relative sea-level fall that may be associated with drier conditions with less rainfall during the second part of the last millennium. As suggested by this work, slight relative sea-level fluctuations caused by regional or global climatic change may affect significantly the current mangrove area.

1. Introduction

Recent works focusing the evolution of Amazonian mangroves have documented an expansion during the early and middle Holocene, followed by their replacement by freshwater vegetation along the Marajó Island coast in areas in the Amazon River mouth (Cohen et al., 2012; Rossetti et al., 2012). Mangroves and salt-marsh vegetation persisted in areas with marine-influenced littoral, where brackish water vegetation is recorded over tidal mud flats throughout the Holocene. A hypothesis has been raised which considers the fragmentation of this mangrove belt during the late Holocene as caused by the increase in freshwater discharge associated with changes from dry into wet climates in the late Holocene (Cohen et al., 2012; França et al., 2012; Guimarães et al., 2012, 2013a, 2013b; Smith et al., 2012).

The Amazon River's discharge supplies about 20% of the particulate flow reaching the coast in the form of shoreface-attached mud banks that tend to evaluate to tidal mud flats (ANA, 2003; Gallo and Vinzon, 2005; Allison et al., 1995). Apparently, the deposition of muddy sediments and fluvial discharge were not constant during the late Holocene (e.g. Sommerfield et al., 2004; Cohen et al., 2012; Guimarães et al., 2012, 2013a, 2013b), and changes in the river discharge may result in significant relative sea-level variations along the coast (e.g. Mörner, 1996, 1999). Therefore, at a regional level, rapid marine regressions may be caused by short (century-scale) regional dry events (Mörner, 1999).

There are still few studies about the effects of recent climatic changes on Amazonian coastal ecosystems (Cohen et al., 2005b, 2008). Considering only the last five hundred years, it is knowledge the periodicity and effects of intermittent climatic phenomena such as strong El Niño events and droughts in the Amazon region, which are potentially devastating to the biota of the affected regions and to the human population dependent thereon (Meggers, 1994). Recent studies establish relations between the El Niño/Southern Oscillation (ENSO) in the tropical Pacific and the sea surface temperature (SST) in the South Atlantic, and the climate in South America is significantly influenced by the South Atlantic dipole and southwestern South Atlantic (e.g. Kayano et al., 2013). During the drought of 2010 in Amazonia, the water levels of major Amazon tributaries fell drastically to unprecedented low values. This drought started in early austral summer during El Niño and then was intensified because of the warming of the tropical North Atlantic, which it was the strongest of the whole 1903–2010 period (Marengo et al., 2011).

The longest calendrical chronology of E1 Niño events has been compiled from observations of rainfall on the coast of Peru during the past 500 years (Quinn et al., 1987). ENSO events prior to 1500 AD may be indicated by extrapolations from tree-rings, ice cores, flood deposits, beach ridges, varved sediments, mollusk fauna, river levels, and coral

* Corresponding author at: Laboratory of Coastal Dynamics, Graduate Program of Geology and Geochemistry, Institute of Geoscience, Federal University of Pará (UFPA), Rua Augusto Correa 01, 66075-110 Belém, PA, Brazil.
E-mail address: mcohen@ufpa.br (M.C.L. Cohen).

http://dx.doi.org/10.1016/j.catena.2015.06.012
0341-8162/

growth (Diaz and Markgraf, 1992; Enfield, 1992; DeVries, 1987). Additionally, archeological discontinuities ca. 1500, 1000, 700, and 400 B.P. may reflect paleoENSO events with a periodicity of approximately 500 years (Lamb, 1988; Sandweiss, 1986; Meggers, 1994).

Little is known about the impacts of mega El Niño on Atlantic estuaries, including the interactions between Amazon discharge and the mangrove vegetation in the last centuries. This issue is particularly relevant to forecast the future evolution of major ecosystems for the next decades to centuries. In addition to the climatic hypothesis, the tectonics may be considered as a possible influencing factor by the relative sea-level affecting the mangrove dynamics at the Amazon mouth (e.g. Rossetti et al., 2007).

In order to discuss the relationship between the Amazonia mangrove dynamics and the driving forces that may control the relative sea-level during the last five hundred years, this work presents a detailed description of a sediment core sampled from a herbaceous flat currently not flooded by the tides of the Amapá coast using sedimentary facies, geochemistry, mineralogy, palynology, $\delta^{13}C$, $\delta^{15}N$, C/N and radiocarbon data. In addition, these data are compared with previous work (Cohen et al., 2005a, 2009; Lara and Cohen, 2009, Fig. 1) about the mangrove dynamics along the Pará littoral during the past thousand years.

2. Study area

2.1. Geological setting

The regional geology of the State of Amapá, where the study area is located, includes Mesoarchean–Devonian Crystalline and Metassedimentary rocks of the Amapá Hills to the west, and Pleistocene sandstones and conglomerates in the coastal plateau to the east, the latter representing tidal depositional systems (Souza and Pinheiro, 2009). From the Late Pleistocene to Holocene, erosional and depositional processes due to climatic and sea-level changes, added to tectonic processes, shaped the relief of the Amapá coast (Lima et al., 1991). Extensive north–south trending Holocene terraces composed of sand and mud developed along the coastal plain adjacent to the Amazon River mouth. According to Guimarães et al. (2013a, 2013b), this coastal plain includes muddy and mixed tidal flats with elongated muddy bars, as well as modern and abandoned tide-dominated rivers, lakes, and cheniers (Fig. 1b, c).

2.2. Vegetation

Floristic studies in the coastal plain of the State of Amapá described geobotanical and land use units (Costa Neto, 2004; Costa Neto and Silva, 2004; Carvalho et al., 2006; Costa Neto et al., 2007). For the study site (Fig. 1b, c), a vegetation survey based on qualitative descriptions was carried out (Guimarães et al., 2013a, 2013b). The modern vegetation is mainly characterized by herb vegetation in supratidal areas, "várzea" (flooded freshwater forests on inter and supratidal flat), and mangrove (flooded brackish water forest located on intertidal flat).

2.3. Climate and hydrology

The Atlantic Intertropical Convergence Zone (ITCZ) records the boundary between the southeast and northeast Atlantic trade winds and is associated with a zonal band of low pressure and high precipitation that takes place over both the ocean basin and the South American continent (Peterson and Haug, 2006). The seasonal migration of the ITCZ plays a major role in controlling the patterns of rainfall over the northern coast of South America as it transports moist air from the Atlantic Ocean to the continent (e.g., Poveda and Mesa, 1997). Therefore, the climate of the study site is humid tropical characterized by well-defined dry (September to December) and wet (January to July) seasons, with annual average precipitation and temperature around 3000 mm and 27.5 °C, respectively (Bezerra et al., 1990).

The mean discharge of the Amazon River is approximately 170,000 m^3/s (at the town of Óbidos), with maximum and minimum outflows of 270,000 and 60,000 m^3/s at wet and dry seasons, respectively

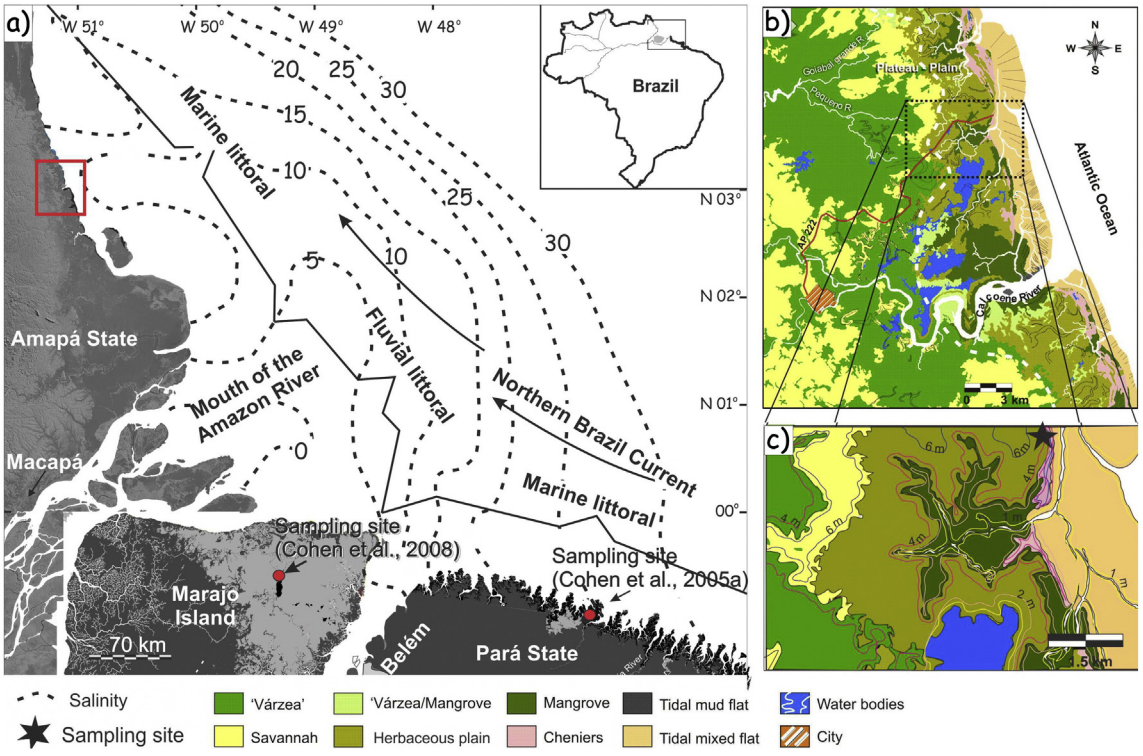

Fig. 1. Study site. a) the northern Brazilian marine and fluvial influenced littoral (modified from Cohen et al., 2012); b) modern geomorphology and vegetation units on the northern Amapá littoral (modified from Guimarães et al., 2013a, 2013b); c) topography and vegetation units of the sampling point.

(ANA, 2003). This discharge contributes with ~1.2×10^9 tons/year of sediment (Meade et al., 1985). However, new mean outflow estimation is approximately 203,000 m^3/s and sediment discharge about 754×10^6 tons/year (Martinez et al., 2009). The Amazon estuary is classified as semidiurnal macrotidal (Pugh, 1987), with a tidal range of 4 to 6 m (Gallo and Vinzon, 2005).

The Amapá coast appears to be the location of mud banks generation for the entire northeastern coast of South America (Allison et al., 2000). These mud banks are spaced at intervals of 15 to 25 km separated by inter-bank areas, are up to 5 m thick, 10 to 60 km long and 20 to 30 km wide, and migrate along the Amazon-influenced muddy coast from 1 to >5 km/year (Gardel and Gratiot, 2005) in water depths of <5 to 20 m over a modern upper shoreface mud wedge created from deposition of previous mud banks (Allison et al., 2000).

The sediments that escape from Amazon shelf are transported in turbid suspension (suspended-sediment concentration > 1 g/l) along the coastal zone. These mechanisms transport an amount equivalent to about 15–20% of the Amazon sediment outflow (Wells and Coleman, 1978; Eisma et al., 1991). Sediment input by local rivers (~20 tons/year; Eisma and Van der Marel, 1971) is much smaller than the Amazon contribution (Eisma and Van der Marel, 1971; Gibbs, 1976). Storm events are absent in this equatorial setting, which increases the relative importance of seasonal meteorological and fluvial variations in regulating sediment flux to this muddy coast (Allison et al., 2000).

The structure of the plume is controlled by the North Brazilian Current, which induces a northwestern flow with speeds of 40–80 cm/s over the continental shelf (Fig. 1b; Lentz, 1995), strong tidal currents (Beardsley et al., 1995), trade winds and the ITCZ (Lentz and Limeburner, 1995). Consequently, the river discharge and hydrodynamic conditions allow a strong reduction of water salinity along the Amazon River and adjacent coast (Fig. 1b; Vinzon et al., 2008; Rosario et al., 2009).

Then, climatic and hydrological factors have mainly controlled the geobotanical units of the Amazon coast leading to the formation of: 1) a fluvial sector, close to the Amazon River mouth, with tidal water salinity below 7‰, characterized by *várzea* and herbaceous vegetation; and 2) a marine-influenced littoral, submitted to tidal water salinity between 30‰ and 7‰ (southeastern and northwestern coastline) and dominated by mangroves and salt-marsh vegetation (Fig. 1a, Cohen et al., 2012).

Regarding the marine influenced littoral of the Amapá, the increase in rainfall during the wetter period is well-correlated with the increase of the Calçoene River discharge (Fig. 1b) and expansion of the tidal influence on upper surface. Considering this tidal water salinity is yet suitable to the mangrove development, this process favors the development of mangroves on muddy substrates near the coastline (Guimarães et al., 2013a, 2013b).

3. Materials and methods

3.1. Remote sensing

The morphological aspects of the study area were characterized based on the analysis of Landsat images 5-TM, obtained in September 1997 by the Brazilian National Institute for Space Research-INPE (for details about the image processing see Guimarães et al., 2013a, 2013b). The topographic profile is based on the digital elevation model acquired during the Shuttle Radar Topography Mission-SRTM undertaken by the National Aeronautics and Space Administration-NASA. The software Global Mapper 9 (Global Mapper LLC, 2009) was used to process the topographic data (Fig. 1c).

3.2. Sampling and facies description

The sedimentary record consisted of a 1 m deep-core sampled from a herbaceous flat not flooded by tide (02°36′52″N, 50°50′41″, Fig. 1c). The core was drilled near the city of Calçoene using a Russian Sampler with the geographical and topographical positions obtained from the digital elevation model based on SRTM and Landsat/TM data analyses presented by Guimarães et al. (2013a, 2013b). Facies analysis included descriptions of color, lithology, texture and structures (cf. Walker, 1992). X-ray radiographs aided the identification of sedimentary structures. The sedimentary facies was codified following Miall (1978).

3.3. Mineralogical and chemical analyses

The identification of minerals was achieved using X-ray powder diffraction by a PANalytical diffractometer model PW 3040, with a copper anode (kα1 = 1.54060 Å), tension generator and current adjusted to 40 kV and 30 mA, respectively. Records were obtained in the range of 5 to 75° 2θ, with step size 0.02–10 s. The results were interpreted using X'Pert HighScore 2.1 software and the International Center for Diffraction Data database, and are presented as mineral symbols following Kretz (1983) and Spear (1993).

The chemical composition was analyzed from a 0.2 g sample by Inductively Coupled Plasma Optical Emission Spectrometry (ICP-OES) following lithium metaborate/tetraborate fusion and dilute nitric digestion on an Acme Analytical Laboratory. Total sulfur (TS) and total organic carbon (TOC) were obtained from a LECO CS-300 combustion analyzer.

The contents of major and trace elements were normalized to the Upper Continental Crust — UCC (Wedepohl, 1995) and Post-Archean Australian Shales — PAAS (Turekian and Wedepohl, 1961; Taylor and McLennan, 1985). The data similarity analysis was performed by Single Linkage and Pearson product–moment correlation coefficient (PPCC, denoted by ρ):

$$\rho = \frac{\sum_{i=0}^{n}(xi-\overline{x})(yi-\overline{y})}{\sqrt{\sum_{i=0}^{n}(xi-\overline{x})^2} * \sqrt{\sum_{i=0}^{n}(yi-\overline{y})^2}} = \frac{\mathrm{cov}(X,Y)}{\sqrt{\mathrm{var(X)} * \mathrm{var(Y)}}}$$

where:

P = 1 perfect positive correlation between *x* and *y*.
ρ − 1 perfect negative correlation between *x* and *y*.
ρ = 0 *x* and *y* are not linearly dependent.

3.4. Pollen and spore analyses

1 cm^3 of sediments were picked in 5 cm intervals. One tablet of exotic *Lycopodium* spores was added to each sample for the calculation of pollen concentration (grains/cm^3). All samples were prepared using standard techniques of pollen analysis including acetolysis (Faegri and Iversen, 1989). Handbooks of pollen and spores morphology were consulted (Roubik and Moreno, 1991; Colinvaux et al., 1999; Hesse et al., 2008) to identify pollen grains and spores. Samples were counted to a minimum of about 300 pollen grains. The total pollen sum excludes algae, micro-foraminifers, fungal and fern spores. Pollen and spore data are presented in pollen diagrams as percentages of the total pollen amount. Thirty pollen taxa were identified, but the pollen diagram show only the most abundant pollen taxa (>5% pollen sum) and the different ecological groups (Fig. 3). Taxa were grouped into Mangrove, Herbaceous plain, and "Várzea". Regarding the significant changes of sedimentation rates along the cores sampled from tidal flats, which it causes changes in pollen concentrations, and consequently a misinterpretation of the pollen profile, we used percentages of pollen grains along the studied core. The softwares Tilia and Tilia Graph were used to the calculation and plotting of pollen diagrams. The pollen diagrams were statistically subdivided into zones of pollen and spores assemblages based on square-root-transformation of the percentage data and stratigraphically constrained cluster analysis by the method of total sum of squares (Grimm, 1987).

3.5. C/N, carbon and nitrogen isotopes

The $\delta^{13}C$, $\delta^{15}N$ and elementar C and N (C/N) amounts were analyzed from sediment samples (6–50 mg) taken at 5 cm intervals along the sedimentary facies. The stable carbon and nitrogen isotopes as well as the total organic carbon (TOC) and nitrogen (TN) were determined at the Stable Isotopes Laboratory of Center for Nuclear Energy in Agriculture (CENA), University of Sao Paulo (USP), using a Continuous Flow Isotopic Ratio Mass Spectrometer (CF-IRMS). Organic carbon and nitrogen are expressed as percentage of dry weight and ^{13}C results are given with respect to VPDB standard and atmospheric N_2, respectively, using the conventional δ (‰) notation. Analytical precision is $\pm 0.1\%$ and ± 0.2‰, respectively.

The organic matter source will be environment-dependent with different $\delta^{13}C$, $\delta^{15}N$ and C/N compositions (e.g. Lamb et al., 2006), as follows: The C_3 terrestrial plants shows $\delta^{13}C$ values between −32‰ and −21‰ and C/N ratio > 12, while C4 plants have $\delta^{13}C$ values ranging from −17‰ to −9‰ and C/N ratio > 20 (Deines, 1980; Meyers, 1997). Freshwater algae have $\delta^{13}C$ values between −25‰ and −30‰ (Meyers, 1997; Schidlowski et al., 1983) and marine algae around −24‰ to −16‰ (Meyers, 1997). Thornton and McManus (1994) and Meyers (1997) used $\delta^{15}N$ values to differentiate organic matter from aquatic (>10.0‰) and terrestrial plants (~0‰).

3.6. Radiocarbon dating

Two bulk samples of ~2 g each were used for radiocarbon dating (Table 1). The sediment samples were checked and physically cleaned under the microscope. The residual material was then extracted with 2% HCl at 60 °C during 4 h, washed with distilled water until neutral pH and dried (50 °C). The samples were analyzed by Accelerator Mass Spectrometry (AMS) at the Center for Applied Isotope Studies (Athens, Georgia, USA). Radiocarbon ages are reported in years before AD 1950 (yr BP) normalized to $\delta^{13}C$ of −25‰VPDB and in cal yr BP with a precision of 2σ (Reimer et al., 2004).

4. Results

4.1. Radiocarbon date and sedimentation rates

The radiocarbon dates are shown in Table 1 and no age inversions were observed. The sedimentation rates were based on the ratio between the depth intervals (mm) and the time range. The calculated sedimentation rates are 0.13 mm/years (100–30 cm) and 0.67 mm/years (30–0 cm). Although the rates are nonlinear between the dated layers, they are the same magnitude order with the vertical accretion range of 0.1 to 10 mm yr^{-1} of mangrove forests reported by other authors (e.g. Cahoon and Lynch, 1997; Bird, 1980; Spenceley, 1982; Behling et al., 2004; Cohen et al., 2005a, 2008, 2009; Guimarães et al., 2010; Vedel et al., 2006).

4.2. Facies descriptions

The bulk of the sediment record consists of bioturbated muds. Pollen and spore records, $\delta^{13}C$, $\delta^{15}N$ and C/N values were added to facies characteristics in order to define two environments, which include mangrove and herbaceous plain.

Table 1
List of radiocarbon dates (AMS) calibrated by CALIB 5.1 Beta (Reimer et al., 2004).

Sample ID	Lab. number	Depth (cm)	Radiocarbon age (yr B.P.)	2σ calibration (cal yr B.P.)
G1 30	UGAMS 8201	30	320 ± 30	470–310
G1 100	UGAMS 8196	100	4810 ± 40	5610–5470

4.2.1. Mangrove facies

The mangrove facies is present at the base of the studied core (5610–5470 cal yr BP until 470–310 cal yr BP). It consists of mud with abundant roots, root marks and dwelling structures produced by the benthic fauna (Fig. 2).

This facies corresponds to the G1A palynological zone that is mainly composed by *Avicennia* (5–75%) and *Rhizophora* (5–30%), characterizing the mangrove vegetation. The herbaceous plain is mainly represented by Poaceae (20–70%) and Cyperaceae (0–35%), while the *várzea* forest is mainly characterized by Papilionoideae (0–20%), Mimosoideae (0–20%), Pseudobombax (0–13%), Ilex (0–10%) and Mauritia (0–10%) (Fig. 3a).

The sediment $\delta^{13}C$ values ranging between −23.2‰ and −25‰ suggest the contribution of C_3 plants, probably associated with marine and freshwater organic matters. The $\delta^{15}N$ values (1.3‰ to 5‰) indicate a mixture of terrestrial and aquatic influences. The C/N values between 5 and 10 are consistent with a higher influence of aquatic organic matter (<10 algae dominance and > 12 vascular plants; Meyers, 1994; Tyson, 1995) (Fig. 3b). The relationship between $\delta^{13}C$ and C/N confirms the contribution of marine and freshwater organic matters (Fig. 4).

4.2.2. Herbaceous plain facies

This facies occurs in the upper segment of the G1 site from 470 to 310 cal yr BP until the present. It presents mud with many fine root marks, herbaceous roots and oxidized features (Fig. 2). Pollen assemblages are dominated by herbaceous plain pollen and correspond to Zone G1B that is represented by Poaceae (40–75%) and Cyperaceae (15–30%) pollen. Monolete (50–70%) and trilete psilate (0–50%) spores also occur in relatively high percentages (Fig. 3a).

The relationship between $\delta^{13}C$ (−21.5‰ to −23‰) and C/N (11–15) (Fig. 3b) suggests contribution of C_3 plants (−32‰ to −21‰; Deines, 1980) (Fig. 4). The $\delta^{15}N$ (−0.8‰ to 1.5‰) (Fig. 3b) values indicate higher influence of terrestrial organic matter than the mangrove facies.

4.3. Distribution of minerals, major and trace components along the mangrove and herbaceous plain facies

The minerals included quartz, kaolinite, anatase, muscovite, albite and K-feldspar. The major components were SiO_2 (59–65%), Al_2O_3 (15–17%), Fe_2O_3 (5–8, 6%), K_2O (2.3–2.6%), MgO and Na_2O (1.2–1.5%), TiO_2 (~0.8%), CaO (0.4–0.6%), P_2O_5 (~0.1%) and MnO (0.3%) (Fig. 5). In general, the trace elements occurred in a homogeneous pattern along the G1 core, except for Ba and Sr that slightly decreased from the mangrove to the herbaceous plain facies. Total organic carbon and sulfur were found at low concentrations (~0.3% and 0.05%, respectively) in the mangrove facies, slightly increasing to 1.3% and 0.7%, respectively, in the herbaceous plain facies.

The correlation coefficient between SiO_2/Al_2O_3 (−0.72) indicates a quartz/clay antagonism. Additionally, the coefficient between SiO_2/Zr (0.78) indicates the presence of zircon in the sand fraction of the sediment. SiO_2 and Al_2O_3 are the most abundant components, comprising quartz, diatom shells (Costa et al., 2004) and clay minerals (kaolinite). The slight upward depletion of Na_2O, MgO, CaO, Ba and Sr from the mangrove to the herbaceous plain facies likely indicates a decrease in sea water influence. The high contents of Fe_2O_3 and weak coefficient between Fe_2O_3/Cr (0.44) and Fe_2O_3/total sulfur (−0.04) are consistent with iron oxyhydroxides, most likely goethite, as suggested by the yellowish hues, formed during prolonged subaerial exposure, especially observed in the herbaceous plain facies (Berrêdo et al., 2008).

The presence of albite and muscovite indicates a contribution of Precambrian crystalline rocks from the Guiana Shield, which occurs near the coastal plain of the State of Amapá (Guimarães et al., 2013a, 2013b). Other studies focused on the tidal flats of the northern Brazilian coast have also shown the predominance of quartz and kaolinite, but also with occurrences of smectite, illite, pyrite, jarosite, halite,

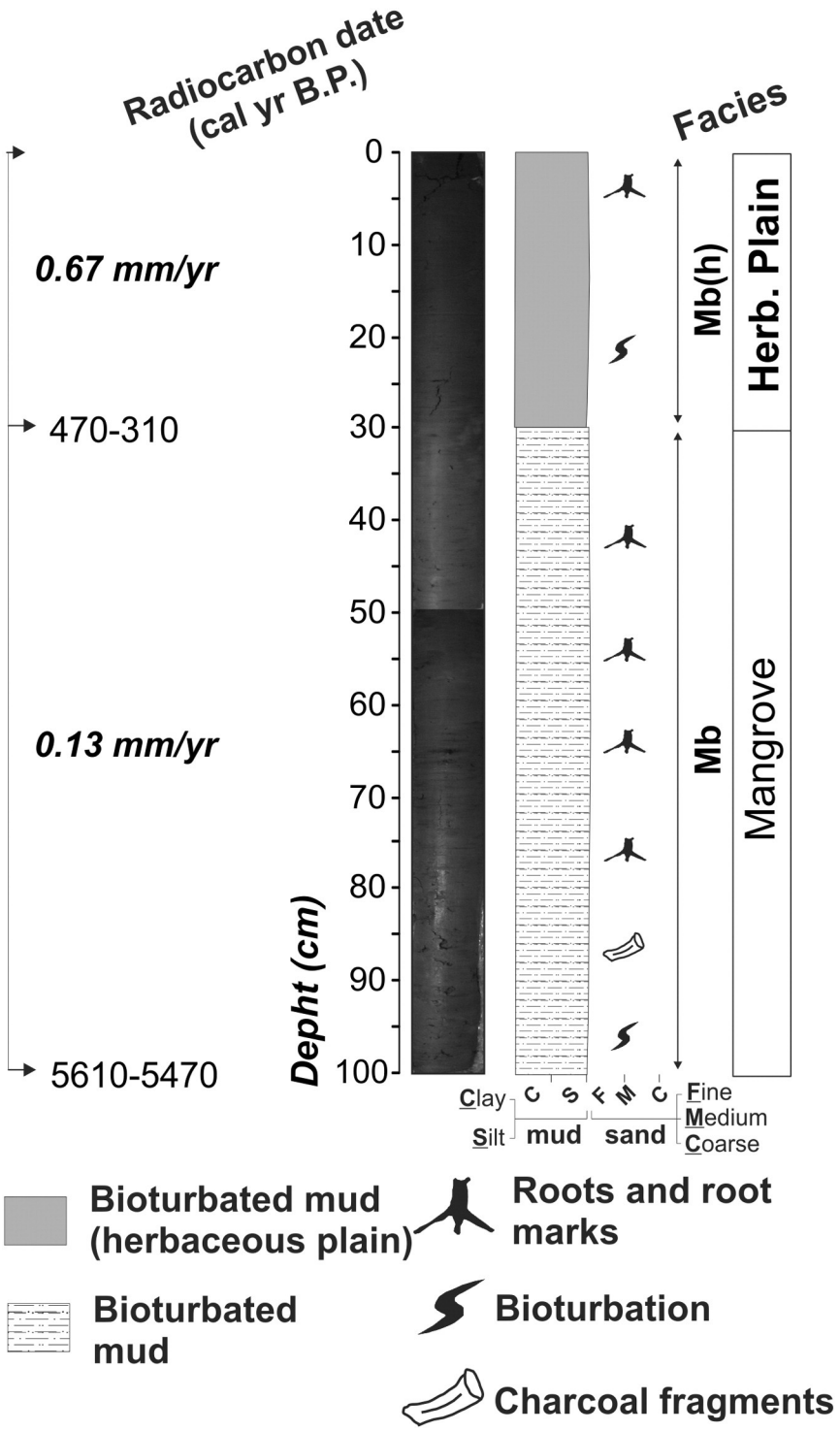

Fig. 2. Sedimentary data from the study core.

muscovite, feldspar, albite, vermiculite and vermiculite–chlorite (Costa et al., 2004; Berrêdo et al., 2008; Vilhena et al., 2010).

5. Discussion

Mangroves are considered as indicators of coastal changes (e.g. Blasco et al., 1996) as the development of mangroves is controlled by land–ocean interaction (e.g. Woodroffe, 1982; Cohen et al., 2005b), and their expansion is determined by the topography of the pre-Holocene sediment surface and prevailing wave and current energy conditions (Woodroffe, 1982). The mangrove community is often strikingly zoned parallel to the shoreline, with a series of different species dominating from open water to the landward margins (Snedaker, 1982). These zones are the response of individual mangrove species to the gradients of tidal inundation frequency, nutrient availability, soil salt concentration across the intertidal area, substrate types, and sediment and freshwater delivery (e.g. Hutchings and Saenger, 1987; Wolanski et al., 1990; Semeniuk, 1994; Lara and Cohen, 2006). An empirical model based on an ecohydrological approach, which allowed the integration of hydrographical, topographical and physicochemical

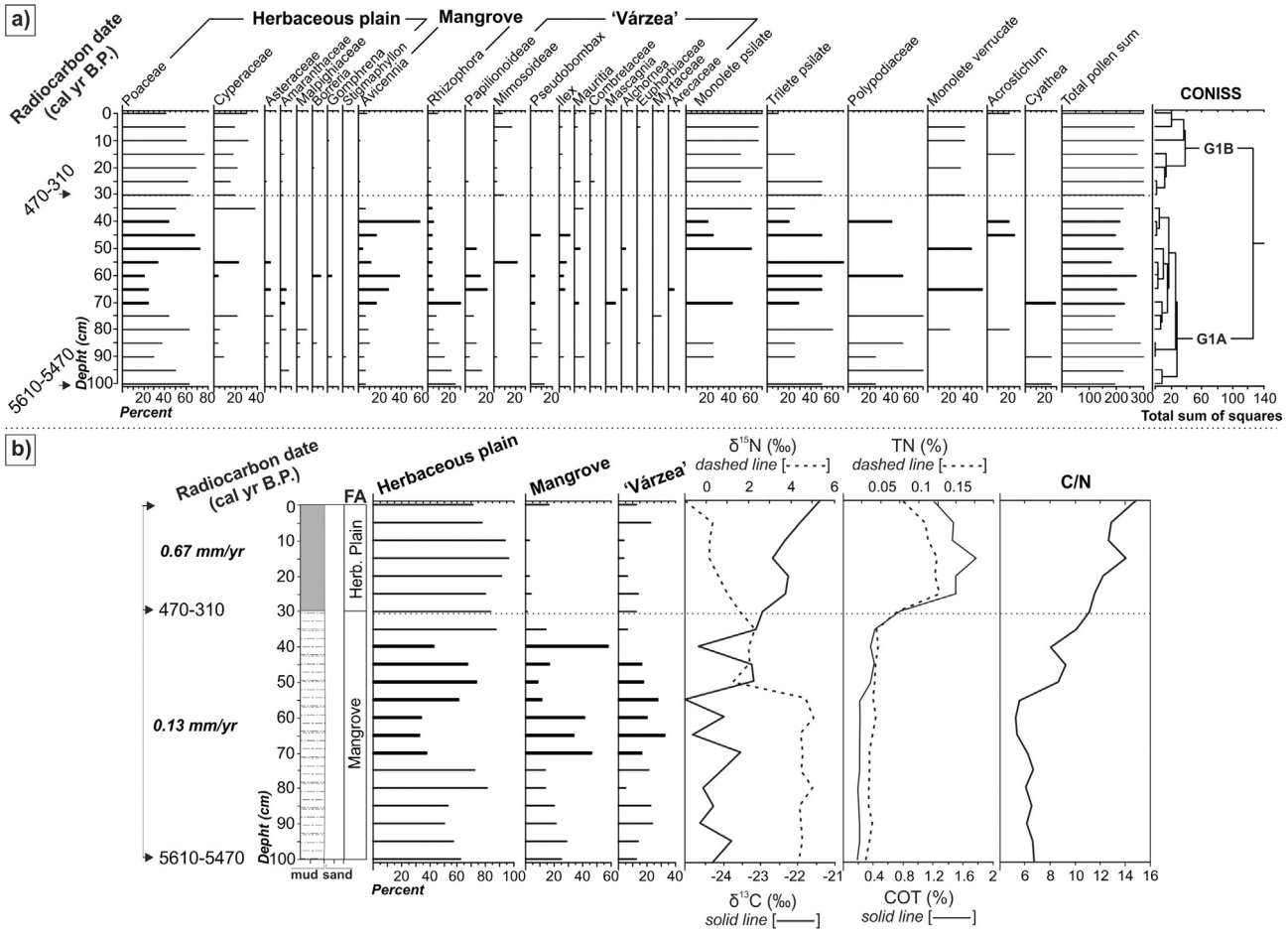

Fig. 3. Integrated graphics, (a) pollen diagram and (b) interproxy records.

information with vegetation characteristics of mangroves and marshes, indicates that changes in pore water salinity are displacing the vegetation boundaries (Cohen and Lara, 2003; Lara and Cohen, 2006).

Several studies based on mangrove development around mean sea-level have proposed historical sea level fluctuations (e.g. Scholl, 1964; Fujimoto et al., 1996; Beaman et al., 1994; Woodroffe et al., 1993; Fujimoto and Miyagi, 1993; Bryant et al., 1992; Chappell, 1993; Caratini and Fontugne, 1992; Clark and Guppy, 1988; Mildenhall and Brown, 1987; Cohen et al., 2005a, 2012).

Considering the present Amazonian mangrove development between 1 and 3.3 m above the mean sea-level (amsl) (Cohen et al., 2005a; Guimarães et al., 2013a, 2013b), it is reasonable to suggest that the mud deposits mostly with mangrove pollen were formed in a mangrove forest within the tidal zone where the modern mangrove is currently under development. The studied core was sampled from an herbaceous flat not flooded nowadays by tide (~3.6 m amsl, Fig. 1c), and the data indicate that mangroves have occurred continually over tidal mud flats with marine influence between >5610–5470 and

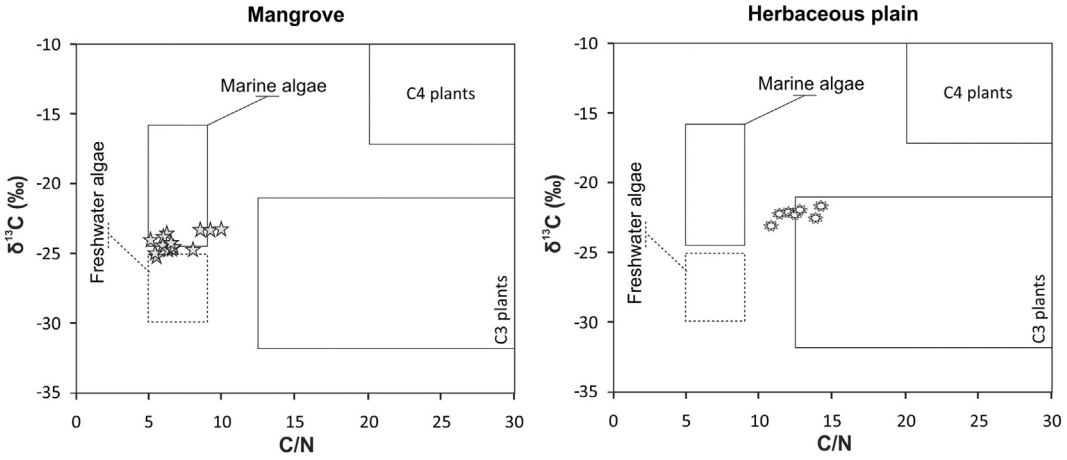

Fig. 4. Binary diagram between $\delta^{13}C \times C/N$ for the mangrove and herbaceous field facies.
Modified from Meyers, 1997; Lamb et al., 2006).

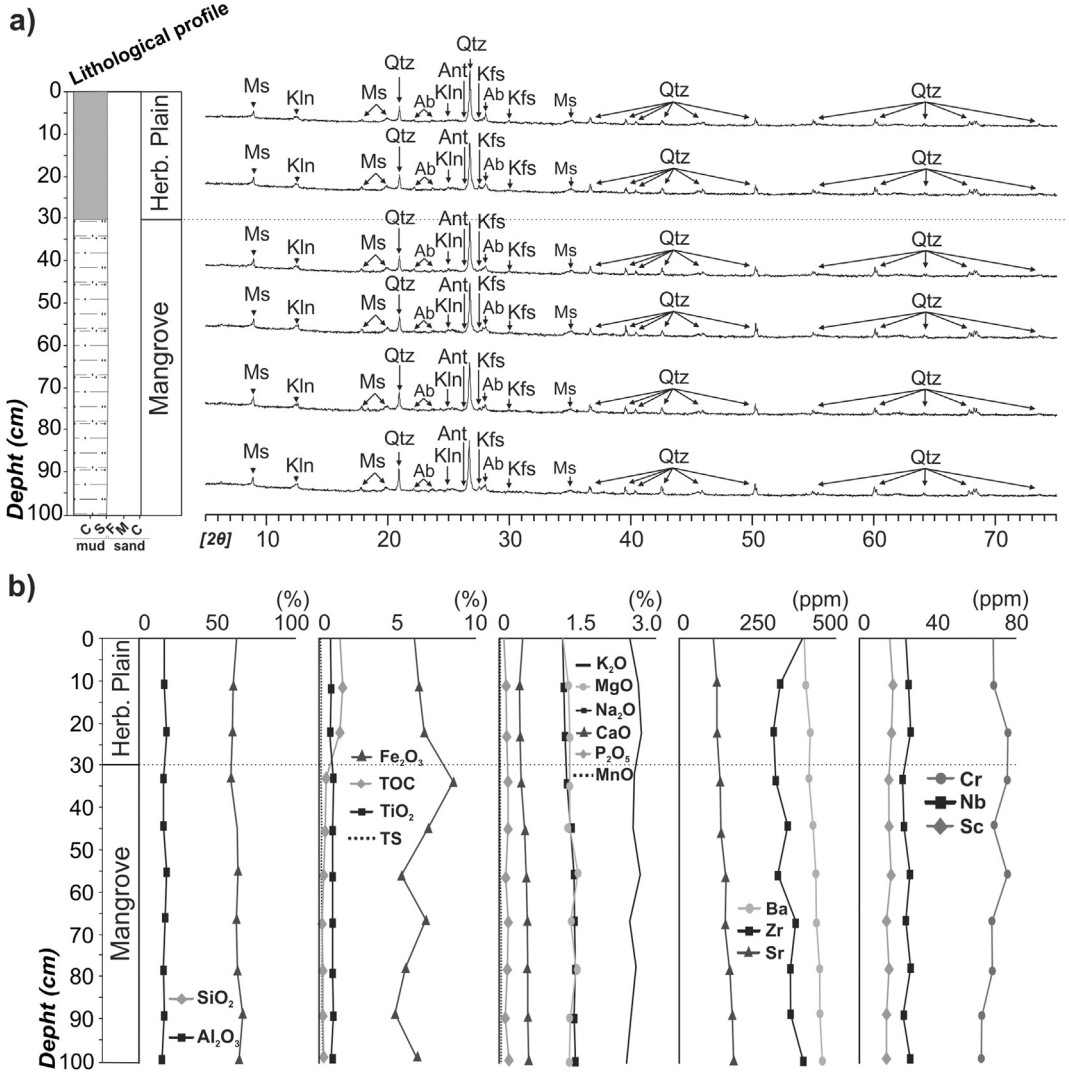

Fig. 5. Mineralogical and chemical compositions of the studied core.

470–310 cal yr BP. The absence of mangrove vegetation since 470–310 cal yr BP is followed by the transition of brackish water organic matter to terrestrial C_3 plants (Figs. 3 and 4). Besides, the geochemical analyses indicate a decrease in sea–water influence during the last centuries (Fig. 5). Then, based on the main physical and chemical parameters controlling the mangrove presence, we present three possible interpretations for the change from mangrove to herbaceous vegetation at about 470–310 cal yr BP.

5.1. Tidal-influenced paleochannel

Decreasing water energy during the abandonment of tidal-influenced channels might lead to the disappearance of mangrove due to its replacement by *várzea* or gallery forest at channel margins. A study undertaken in the nearby Marajó Island showed that when channels are fully abandoned and filled with sediment, the channel surface is occupied first by grasslands and ultimately by *terra-firme* forest (Rossetti et al., 2010). However, the sampling site does not present an elongated and sinuous morphology above high-water level that may suggest channel abandonment. The geomorphological map (Fig. 1b and c) suggests that the sampling site, positioned on a topographically elevated surface not influenced by modern tides, was a wide tidal plain.

5.2. Normal marine regression

According to Posamentier et al. (1992), the term "regression" describes a retreat of the sea and a concomitant seaward expansion of the land. Regression can occur when sufficient sediment is entering into the coastal system so as to overwhelm the amount of space available. This can occur during stillstands or rises in relative sea-level, and is referred to as a "normal" regression. In this case, the mudflat may be no longer affected by brackish water, and, consequently the mangroves migrate to a lower topographic position, as suggested by the topography and vegetation map of the studied core (Fig. 1c).

5.3. Forced marine regression

When no sediment is delivered to the shoreline during a relative sea-level fall, the regression is said to be forced because a seaward shift of the shoreline must occur, even if the volume of sediment supplied is low. This is in marked contrast to "normal" regression, which occurs in response to the balance between variations of sediment flux and new space added (Posamentier et al., 1992). In this situation, the change from mangrove to herbaceous vegetation at about 470–310 cal yr BP (~1560 AD) may be a consequence of a decrease of marine influence caused by a gradual relative sea-level fall, in agreement with the relative sea-level curve published by Cohen et al. (2005a) (Fig. 6).

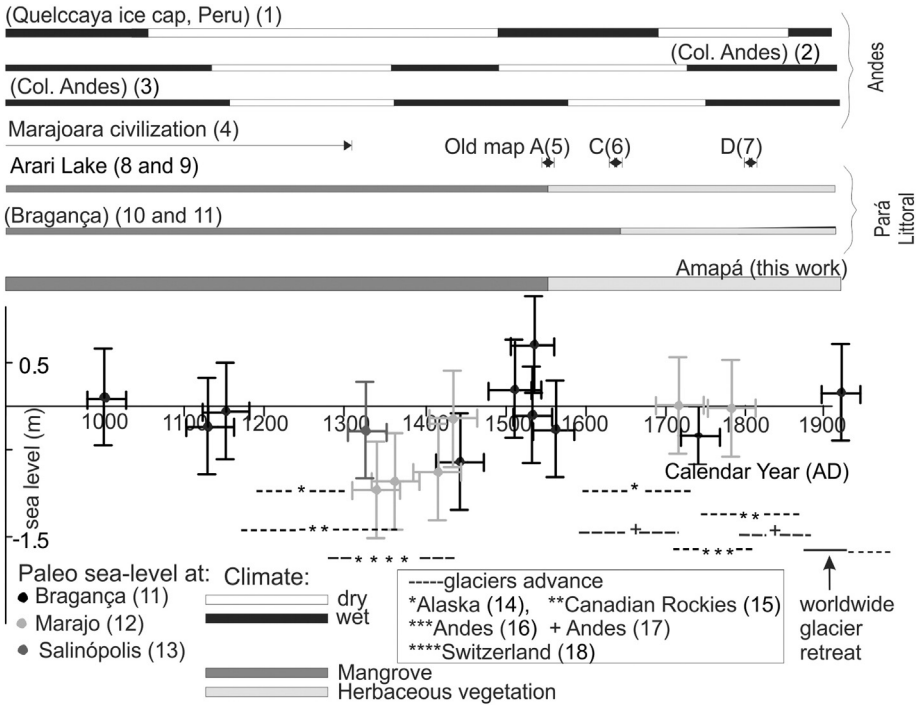

Fig. 6. Comparative diagram of the climatic change records from South America and relative sea-level curve for Pará Littoral, and the mangrove/herbaceous succession in Amapá and Pará littoral over the past 1000 years. After Cohen et al. (2009). References: (1) Thompson et al. (1985), (2) Eisma et al. (1991), (3) Van der Hammen (1986), (4) Roosevelt (1991), (5) Gutiérrez (1562), (6) Teixeira (1630), (7) Arrowsmith (1811), (8) Lara and Cohen (2009), (9) Cohen et al. (2008), (10) Behling et al. (2001), (11) Cohen et al. (2005a), (12) Behling et al. (2004), (13) Cohen et al. (2009), (14) Calkin et al. (2001), (15) Luckman (2000), (16) Iriondo and Kröhling (1995), (17) Solomina et al. (2007), (18) Röthlisberger et al. (1980).

5.3.1. Relative sea-level and tectonics

Nowadays, some sectors of the Amapá and Pará littoral present phases of expansion and contraction of mangrove areas, due to changes in the relative sea-level (Cohen and Lara, 2003; Cohen et al., 2009; Guimarães et al., 2013a, 2013b). Considering the recent decadal relative sea-level rise, the marine littoral shows landward displacement of mangrove over topographically higher herbaceous sectors (Cohen and Lara, 2003; Cohen et al., 2009).

The tectonics may be analyzed as a possible factor influencing the relative sea-level and consequently the dynamics of mangrove environments at the Amazon mouth. This is suggested because this area is located in a geological setting that was reactivated tectonically in the late Holocene (Rossetti et al., 2007), a process that might continue going on at Present based on the fact that this is one of the eight seismogenic zones of the Amazonia with recorded earthquakes up to 4.8 of magnitude (Miotto, 1993). A previous work has proposed that the changes in the mangrove environment in Marajó Island occurred simultaneously with the transformation of an embayed coast into a coast with rectilinear morphology (Rossetti et al., 2012). According to these authors, this morphological modification occurred by coastal progradation due to stabilization following a period of tectonic activity that promoted the detachment of this island from mainland. An increasing volume of publications has addressed the role of tectonics in inland areas of northern Brazil during the Neogene and Quaternary (Rossetti et al., 2012). However, there are still few studies about the effects of tectonics on relative sea-level near the Amazonian coast during the last thousand years.

5.3.2. Relative sea-level and climatic changes during the last 500 years

Rainfall changes may have a geographically wider effect on vegetation in northern Brazil (e.g. Van der Hammen, 1974; Absy et al., 1991; Desjardins et al., 1996; Ledru, 2001; Behling and Costa, 2000; Pessenda et al., 2001,2004). Thus, the connection among events recorded in different parts of South America can be attributed to the fluvial system, since river discharge affects mangrove distribution (Cohen et al., 2012). Short (century-scale) regional dry events cause decrease in river discharge, and it may result in significant relative sea-level fall (e.g. Mörner, 1996, 1999).

It has been argued that the decreased river discharges during dry periods in Amazonia causes an upriver mangrove invasion along estuarine valleys due to an upriver increase of estuarine water salinity (Lara and Cohen, 2006; Cohen et al., 2012). This process may also cause a displacement of mangrove forest to lower topographic areas. It may also cause an herbaceous field expansion over previous mangrove area in the marine Amapá littoral (Guimarães et al., 2013a, 2013b), due to the relative sea-level fall generated by the decrease of fluvial discharge.

Data from the Colombian Andes indicate wet and dry periods during the last 800 years (Van der Hammen, 1986), which may have produced changes in the Amazon River discharge (Vital and Stattegger, 2000). Geological studies of the Amazon shelf show changes in the dispersal of Amazon River sediments during the late Holocene (Alexander et al., 1986; Eisma et al., 1991). Erosion of deposits probably occurred between about 1310 AD and the end of the 19th century, when the modern phase of accumulation began, indicating a maximum hiatus of about 600 years. This depositional and erosional phase is due to the interactions of river discharge with oceanographical and meteorological processes (Sommerfield et al., 1995). More specifically, Eisma et al. (1991) suggest that dry climatic periods in the Colombian Andes from 1510 to 1770 AD reduced the supply of Amazon sediment and water to the shelf, resulting in erosion or non-deposition.

These dry periods was attributed to southward displacement of the ITCZ, in which modeling studies have documented a cooling in the Northern Hemisphere, such as observed during the Little Ice Age (LIA) (Zhang and Delworth, 2005; Broccoli et al., 2006). The reconstruction of Pacific SST points toward a La Nina-like state during the Medieval Climate Anomaly and an El Niño-like state during the LIA (Cobb et al., 2003; Graham et al., 2007; Conroy et al., 2008; Mann et al., 2009).

Considering the LIA event between ~1400 and ~1900 AD (Rudddiman, 2008), previous pollen studies in the Pará littoral revealed mangrove migration to lower topography and herbaceous vegetation

expansion at about 1560 AD and 1650 AD, respectively, suggesting a relative sea-level fall (Cohen et al., 2005a, Fig. 6). Following this trend, the east of Marajó Island recorded a relative sea-level fall that may be associated with drier conditions with relatively low fluvial discharge between the 16th and 19th centuries (Lara and Cohen, 2009, Fig. 6). According to these authors, a large portion of the low-lying eastern Marajó Island was probably submerged 500 years ago, at least during high tide, as suggested by maps of the sixteenth century (Gutiérrez, 1562, Fig. 7A). At about 1600 AD, one of the intermittent intense droughts related to strong El Niño events affected Marajó Island (Meggers, 1994). In the seventeenth century, higher sectors of eastern Marajó probably began to emerge as land and several small islands appeared within the current perimeter of the island. This is further supported by Teixeira's detailed map of 1630 (Teixeira, 1630, Fig. 7C), where the current Marajó Island is represented as an archipelago. Land emergence was complete by the end of the eighteenth century. This is supported by a registered stabilization of RSL close to current values (Cohen et al., 2005a) and also by Arrowsmith's map, based on "manuscript maps and surveys made between 1771 and 1806" (Arrowsmith, 1811, Fig. 7D), where the Marajó Island has basically the same morphology as nowadays. This scenario would point to large and rapid changes in the Amazon's mouth, probably reflecting regional effects of global climatic events.

Archeological discontinuities ca. 1500, 1000, 700, and 400 years BP may reflect paleoENSO events, and they must have been substantially more severe than the 1982–83 episode (Lamb, 1988; Meggers, 1994). Several kinds of evidence support this interpretation. Pollen cores from the margins of the forest show replacement by savanna at these times, according to the higher sensitivity of the vegetational boundary to drought (Frost, 1968). Exceptionally low water levels occurred in the Amazon (Moseley et al., 1983; Nials et al., 1979). The probable existence of four episodes of exceptional intensity during the past two millennia suggests a periodicity of approximately 500 years (Sandweiss, 1986). Since the most recent mega-Niño occurred ca. 400 years BP, another can be expected in the coming decades if contributory conditions remain the same (Meggers, 1994).

Regardless the driving force behind the wetland dynamic during the past 1000 years, it is noteworthy that data presented along this work do not mean that mangroves shrank or expanded during the last 500 years. The sediment cores from Bragança Peninsula (Cohen et al., 2005a) and Amapá littoral were sampled from topographically highest sectors of that old tidal plain, where mangroves are most susceptible to relative sea-level fall. These cores only reveal a replacement of mangroves by herbaceous plains, suggesting a mangrove migration to topographically lower areas of tidal flats. Considering the core of Marajó Island, which was sampled from a lake in the center of this island (Cohen et al.,

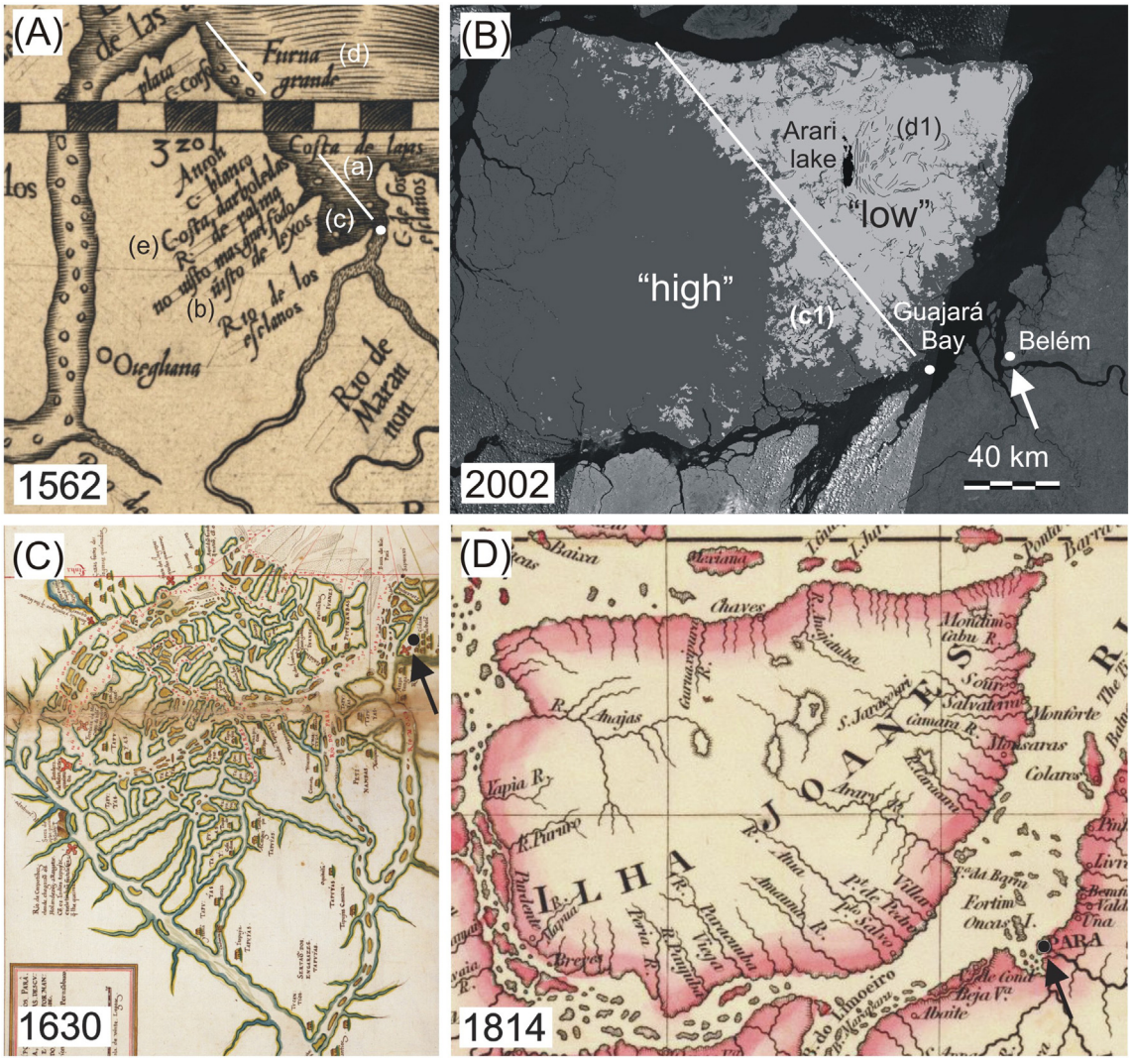

Fig. 7. Evolution of the Marajó Island in the last five centuries after the maps of Gutiérrez (1562) (A), Teixeira (1630) (C), Arrowsmith (1811) (D) and a LANDSAT image (B). The arrow shows the position of the city of Belém in the State of Pará, Brazil (Lara and Cohen, 2009).

2008), probably, the pollen signal recorded the displacement of mangroves following the progradation of coastline caused by the relative sea-level fall. This process caused a decrease in contribution of mangrove pollen inside the lake.

6. Conclusion

The mangroves have occurred continually over tidal mud flats with marine influence in the study site between >5610–5470 and 470–310 cal yr BP. The absence of mangrove vegetation since 470–310 cal yr is followed by transition of sedimentary organic matter sourced from marine/freshwater to terrestrial C3 plants. Besides, the geochemical analysis indicates a decrease in sea water influence during the last centuries. Likely, displacement of mangrove forest to lower surface in the study site was caused by a relative sea-level fall that may be associated with drier conditions with less rainfall during the second part of the last millennium. Therefore, depending mainly on the local topography and fluvial discharge, slight relative sea-level fluctuations caused by regional or global climatic change will affect significantly the current mangrove area. In this context, the definition of potential impacted zones and assess to the intensities and time scales of mega-Niños are fundamental for the coastal vegetation maintenance in addition to its academic importance.

Acknowledgments

We thank the members of the Laboratory of Costal Dynamic (LADIC-UFPA) and Center for Nuclear Energy in Agriculture (CENA-USP). This study was financed by CNPq (Project 473635/2012-7) and by the National Institute on Science and Technology in Tropical Marine Environments — INCT-AmbTropic (CNPq Process 565054/2010-4).

References

Absy, M.L., Clief, A., Fournier, M., Martin, L., Servant, M., Siffeddine, A., Silva, F.D., Soubiès, F., Suguio, K.T., Van der Hammen, T., 1991. Mise em évidence de Quatre phases d'ouverture de la forêt dense dans le sud-est de L'Amazonie au cours des 60,000 dernières années. Première comparaison avec d'autres régions tropicales. C.R. Acad. Sci. Paris 312, 673–678.
Alexander, C.R., Nitrouer, C.A., DeMaster, D.J., 1986. High resolution seismic stratigraphy and its sedimentological interpretation on the Amazon continental shelf. Cont. Shelf Res. 6, 337–357.
Allison, M.A., Nittrouer, C.A., Kineke, G.C., 1995. Seasonal sediment storage on mudflats adjacent to the Amazon River. Mar. Geol. 125, 303–328.
Allison, M.A., Lee, M.T., Ogston, A.S., Aller, R.C., 2000. Origin of Amazon mudbanks along the northeastern coast of South America. Mar. Geol. 163, 241–256.
ANA, 2003. Hydrological information system. Brazilian National Water Agency (On line dataset, 14.3 MB, http://hidroweb.ana.gov.br/baixar/mapa/Bacia1.zip.).
Arrowsmith, A., 1811. Outline of the physical and political divisions of South America. David Rumsey Map collection (http://www.davidrumsey.com/view.html. Cited 10 Mar 2013).
Beaman, R., Larcombe, P., Carter, R.M., 1994. New evidence for the Holocene sea-level high from the inner shelf, Central Great Barrier Reef, Australia. J. Sediment. Res. A Sediment. Petrol. Process. A64 (4), 881–885.
Beardsley, R.C., Candela, J., Limeburner, R., Geyer, W.R., Lentz, S.J., Castro, B.M., Cacchione, D., Carneiro, N., 1995. The M2 tide on the Amazon shelf. J. Geophys. Res. 100, 2283–2319.
Behling, H., Costa, M.L., 2000. Holocene environmental changes from the Rio Curuá record in the Caxiuanã region, eastern Amazon Basin. Quat. Res. 53, 369–377.
Behling, H., Cohen, M.C.L., Lara, R.J., 2001. Studies on Holocene mangrove ecosystem dynamics of the Bragança Peninsula in north-eastern Pará. Brazil. Palaeogeogr. Palaeoclimatol. Palaeoecol. 167, 225–242.
Behling, H., Cohen, M.C.L., Lara, R.J., 2004. Late Holocene mangrove dynamics of the Marajó Island, Amazônia, North Brazil. Veg. Hist. Archaeobot. 13, 73–80.
Berrêdo, J.F., Costa, M.L., Vilhena, M.P.S.P., Santos, J.T., 2008. Mineralogia e geoquímica de sedimentos de manguezais da costa amazônica: o exemplo do estuário do rio Marapanim (Pará). Rev. Bras. Geosci. 38, 26–37.
Bezerra, P.E.L., Oliveira, W., Regis, W.D.E., Brazão, J.E.M., Gavinho, J., Coutinho, R.C.P., 1990. Amazônia legal: zoneamento das potencialidades e dos recursos naturais. Instituto Brasileiro de Geografia e Estatística, Superintendência de Desenvolvimento da Amazônia. Projeto zoneamento das potencialidades dos recursos naturais da Amazônia: geologia, solos e vegetação. Div. 5. Rio de Janeiro, pp. 9–89.
Bird, E.C.F., 1980. Mangroves and coastal morphology. The Victorian Nauralist 97, 48–58.
Blasco, F., Saenger, P., Janodet, E., 1996. Mangrove as indicators of coastal change. Catena 27, 167–178.
Broccoli, A.J., Dahl, K.A., Stouffer, R.J., 2006. Response of the ITCZ to northern hemisphere cooling. Geophys. Res. Lett. 33, L01702.
Bryant, E.A., Young, R.W., Price, D.M., Short, S.A., 1992. Evidence for Pleistocene and Holocene raised marine deposits, Sandon Point, New South Wales. Aust. J. 39, 481–493.
Cahoon, D.R., Lynch, J.C., 1997. Vertical accretion and shallow subsidence in a mangrove forest of southwestern Florida, U.S.A. Mang. Salt Marsh 3, 173–186.
Calkin, P.E., Wiles, G.C., Barclay, D.J., 2001. Holocene coastal glaciation of Alaska. Quat. Sci. Rev. 20, 449–461.
Caratini, C., Fontugne, M., 1992. A high sea level stand assigned to c. 125,000 years BP on the western coast of India. In: Desai, B.N. (Ed.), Oceanography of the indian ocean. Oxford and IBH, New Delhi India, pp. 439–445.
Carvalho, F.P., Costa Neto, S.V., Costa, W.J.P., Coutinho, R.S., Figueira, Z.R., Figueiredo, S.L., Martins, M.H.A., Santos, V.F., Silva, A.Q., Silva, L.M.A., Silva, M.S., Silveira, O.F.M., Takyiama, L.R., 2006. Atlas Zoneamento Costeiro Estuarino do Estado do Amapá. PNMA/SQA/MMA, Macapá 77pp.
Chappell, J., 1993. Contrasting Holocene sedimentary geologies of lower Daly River, northern Australia, and lower Sepik-Ramu, Papua New Guinea. Sediment. Geol. 83, 339–358.
Clark, R.L., Guppy, J.C., 1988. A transition from mangrove forest to freshwater wetland in the monsoon tropics of Australia. J. Biogeogr. 15, 665–684.
Cobb, K., Charles, C.D., Cheng, H., Edwards, R.L., 2003. El Nino/Southern Oscillation and tropical Pacific climate during the last millennium. Nature 424, 271–276.
Cohen, M.C.L., Lara, R.J., 2003. Temporal changes of mangrove vegetation boundaries in Amazonia: application of GIS and remote sensing techniques. Wetl. Ecol. Manag. 11, 223–231.
Cohen, M.C.L., Behling, H., Lara, R.J., 2005a. Amazonian mangrove dynamics during the last millennium: the relative sea-level and the Little Ice Age. Rev. Palaeobot. Palynol. 136, 93–108.
Cohen, M.C.L., Souza Filho, P.W.M., Lara, R.J., Behling, H., Angulo, R.J., 2005b. A model of Holocene mangrove development and relative sea-level changes on the Bragança Peninsula (Northern Brazil). Wetl. Ecol. Manag. 13, 433–443.
Cohen, M.C.L., Lara, R.J., Smith, C.B., Angélica, R.S., Dias, B.S., Pequeno, T., 2008. Wetland dynamics of Marajó Island, northern Brazil, during the last 1000 years. Catena 76, 70–77.
Cohen, M.C.L., Lara, R.J., Smith, C.B., Matos, H.R.S., Vedel, V., 2009. Impact of sea level and climatic changes on the Amazon coastal wetlands during the late Holocene. Veg. Hist. Archaeobot. 18, 425–439.
Cohen, M.C.L., Pessenda, L.C.R., Behling, H., Rossetti, D.F., França, M.C., Guimarães, J.T.F., Friaes, Y., Smith, C.B., 2012. Holocene palaeovironmental history of the Amazonian mangrove belt. Quat. Sci. Rev. 55, 50–58.
Colinvaux, P.A., De Oliveira, P.E., Patiño, J.E.M., 1999. Amazon Pollen Manual and Atlas — Manual e Atlas Palinológico da Amazônia. Hardwood Academic, Amsterdam (332 pp.).
Conroy, J.L., Overpeck, J.T., Cole, J.E., Shanahan, T.M., Steinitz-Kannan, M., 2008. Holocene changes in eastern tropical Pacific climate inferred from a Galapagos lake sediment record. Quat. Sci. Rev. 27, 1166–1180.
Costa Neto, S.V., 2004. Relatório de vegetação: Subsídio ao diagnostico sócio ambiental. Relatório Técnico. IEPA/GERCO, Macapá (32 pp.).
Costa Neto, S.V., Silva, M.S., 2004. Vegetação do setor costeiro estuarino do estado do Amapá. Instituto de Pesquisas Científicas e Tecnológicas do Estado do Amapá. Governo do Estado do Amapá. Cap. 5. Projeto Zoneamento Econômico-Ecológico do setor costeiro estuarino: diagnóstico sócio ambiental participativo do setor costeiro estuarino, pp. 72–96.
Costa, M.L., Behling, H., Berrêdo, J.F., Siqueira, N.V.M., 2004. Mineralogical, geochemical and palynological studies of Late Holocene mangrove sediments from Northeastern Para State, Brazil. Rev. Bras. Geosci. 34, 479–488.
Costa Neto, S.V., Senna, C., Tostes, L.C.L., Silva, S.R.M., 2007. Macrófitas aquáticas das Regiões dos Lagos do Amapá, Brasil. Revista Brasileira de Biociências 5, 618–620.
Deines, P., 1980. The isotopic composition of reduced organic carbon. In: Fritz, P., Fontes, J.C. (Eds.), Handbook of Environmental Isotope GeochemistryThe Terrestrial Environment, A vol. 1. Elsevier, Amsterdam, pp. 329–406.
Desjardins, T., Filho, A.C., Mariotti, A., Chauvel, A., Girardin, C., 1996. Changes of the forest-savanna boundary in Brazilian Amazonia during the Holocene as revealed by soil organic carbon isotope ratios. Oecologia 108, 749–756.
DeVries, T.J., 1987. A review of geological evidence for ancient E1 Niño activity in Peru. J. Geophys. Res. 92, 14471–14479.
Diaz, H.E., Markgraf, V., 1992. El Niño: historical and paleoclimatic aspects of the Southern Oscillation. Cambridge University Press, New York.
Eisma, D., Van der Marel, H.W., 1971. Marine muds along the Guyana Coast and their origin from the Amazon Basin. Contrib. Mineral. Petrol. 31, 321–334.
Eisma, D., Augustinus, P.G.E.F., Alexander, C.R., 1991. Recent and subrecent changes in the dispersal of Amazon mud. Neth. J. Sea Res. 28, 181–192.
Enfield, D.B., 1992. Historical and prehistorical overview of E1 Niño/Southern Oscillation. In: Diaz, H.F., Markgraf, V. (Eds.), El Niño. Cambridge University Press, New York, pp. 95–117.
Faegri, K., Iversen, J., 1989. Textbook of pollen analyses. John Wiley and Sons Ltd., Chichester (328 pp.).
França, M., Francisquini, M.I., Cohen, M.C.L., Pessenda, L.C.R., Rosseti, D.F., Guimarães, J., Smith, C.B., 2012. The last mangroves of Marajó Island — Eastern Amazon: impact of climate and/or relative sea-level changes. Rev. Palaeobot. Palynol. 187, 50–65.
Frost, D.B., 1968. The climate of the Rupununi savannas. Savanna Research. Series 12McGill Univ. Savanna Res. Proj., Montreal.
Fujimoto, K., Miyagi, T., 1993. Development process of tidal-flat type mangrove habitats and their zonation in the Pacific Ocean. A geomorphology study. Vegetatio 106, 137–146.
Fujimoto, K., Miyagi, T., Kikuchi, T., Kawana, T., 1996. Mangrove habitat formation and response to Holocene sea-level changes on Kosrae Island, Micronesia. Mangroves Salt Marshes 1, 47–57.
Gallo, M.N., Vinzon, S., 2005. Generation of over tides and compound tides in Amazon estuary. Ocean Dyn. 55, 441–448.
Gardel, A., Gratiot, N., 2005. A satellite image-based method for estimating rates of mud bank migration, French Guiana, South America. J. Coast. Res. 21, 720–728.
Gibbs, R.J., 1976. Amazon River sediment transport in the Atlantic Ocean. Geology 4, 45–48.
Global Mapper LLC, 2009. Global Mapper Version 9.0 Software (Colorado, Parker).
Graham, N.E., Hughes, M.K., Ammann, C., Cobb, K.M., Hoerling, M.P., Kennett, D.J., Kennett, J.P., Rein, B., Stott, L., Wigand, P.E., Xu, T., 2007. Tropical Pacific-mid-latitude teleconnections during medieval times. Clim. Chang. 81, 241–285.
Grimm, E.C., 1987. CONISS: a FORTRAN 77 program for stratigraphically constrained cluster analysis by the method of the incremental sum of square. Comput. Geosci. 13, 13–35.
Guimarães, José T.F., Cohen, M.C.L., França, M.C., Lara, R.J., Behling, H., 2010. Model of wetland development of the Amapá coast during the late Holocene. Anais da Academia Brasileira de Ciências 82, 451–465.

Guimarães, J.T.F., Cohen, M.C.L., Pessenda, L.C.R., França, M.C., Smith, C.B., Nogueira, A.C.R., 2012. Mid- and late-Holocene sedimentary process and palaeovegetation changes near the mouth of the Amazon River. The Holocene 22, 359–370.
Guimarães, J.T.F., Cohen, M.C.L., França, M.C., Pessenda, L.R., Behling, H., 2013a. Morphological and vegetation changes on tidal flats of the Amazon Coast during the last 5000 cal. yr BP. The Holocene 23, 528–543.
Guimarães, J.T.F., Cohen, M.C.L., França, M.C., Pessenda, L.C.R., Souza, E.J., Nogueira, A.C.R., Alves, R., 2013b. Recent effects of tidal and hydro-meteorological changes on coastal plains near the mouth of the Amazon River. Earth Surf. Process. Landf. 38, 1535–1549.
Gutiérrez, D., 1562. Americae. Library of Congress, Washington, D.C. (http://rs6.loc.gov/ammem/gmdhtml/gutierrz.html. Cited 19 Mar 2013).
Hesse, M., Halbritter, H., Zetter, R., Weber, M., Buchner, R., Frosch-Radivo, A., Ulrich, S., 2008. Pollen terminology: an illustrated handbook. Springer, New York (264 pp.).
Hutchings, P., Saenger, P., 1987. Ecology of mangroves. Queensland University Press (388 pp.).
Iriondo, M., Kröhling, D., 1995. El Sistema Eólico Pampeano. Com. Museo Prov. Cienc. Nat. 5, 1–80.
Kayano, M.T., Andreoli, R.V., Souza, R.A.F., 2013. Relations between ENSO and the South Atlantic SST modes and their effects on the South American rainfall. Int. J. Climatol. 33, 2008–2023.
Kretz, R., 1983. Symbols for rock-forming minerals. Am. Mineral. 68, 277–279.
Lamb, H.H., 1988. Weather, climate and human affairs. Routledge, London.
Lamb, A.L., Wilson, G.P., Leng, M.J., 2006. A review of coastal palaeoclimate and relative sea-level reconstructions using $\delta^{13}C$ and C/N ratios in organic material. Earth Sci. Rev. 75, 29–57.
Lara, J.R., Cohen, M.C.L., 2006. Sediment porewater salinity, inundation frequency and mangrove vegetation height in Bragança, North Brazil: an ecohydrology-based empirical model. Wetl. Ecol. Manag. 14, 349–358.
Lara, R.J., Cohen, M.C.L., 2009. Palaeolimnological studies and ancient maps confirm secular climate fluctuations in Amazonia. Clim. Chang. 94, 399–408.
Ledru, M.P., 2001. Late Holocene rainforest disturbance in French Guiana. Rev. Palaeobot. Palynol. 115, 161–176.
Lentz, S.J., 1995. The Amazon River plume during AMASSEDS: subtidal current variability and the importance of wind forcing. J. Geophys. Res. 100, 2377–2390.
Lentz, S.J., Limeburner, R., 1995. The Amazon River Plume during AMASSEDS: spatial characteristics and salinity variability. J. Geophys. Res. 100, 2355–2375.
Lima, M.I.C., Bezerra, P.E., Araújo, H.J.T., 1991. Sistematização da Geologia do Estado do Amapá. Simpósio de geologia da Amazônia, vol. 3, Belém. Anais. SBG, pp. 322–335.
Luckman, B.H., 2000. The Little Ice Age in the Canadian Rockies. Geomorphology 32, 357–384.
Mann, M.E., Zhang, Z., Rutherford, S., Bradley, R.S., Hughes, M.K., Shindell, D., Ammann, C., Falugevi, G., Ni, F., 2009. Global signatures and dynamical origins of the "Little Ice Age" and "Medieval Climate Anomaly". Science 326, 1256–1260.
Marengo, J.A., Tomasella, J., Alves, L.M., Soares, W.R., Rodriguez, D.A., 2011. The drought of 2010 in the context of historical droughts in the Amazon region. Geophys. Res. Lett. 38, L12703.
Martinez, J.M., Guyot, J.L., Filizola, N., et al., 2009. Increase in sediment discharge of the Amazon River assessed by monitoring network and satellite data. Catena 79, 257–264.
Meade, R.H., Dunee, T., Richey, J.E., et al., 1985. Storage and remobilization of suspended sediment in the lower Amazon River of Brazil. Science 228, 488–490.
Meggers, B.J., 1994. Archaeological evidence for the impact of mega-El Niño events on Amazonia during the past two millennia. Clim. Chang. 28, 321–338.
Meyers, P.A., 1994. Preservation of elemental and isotopic source identification of sedimentary organic matter. Chem. Geol. 114, 289–302.
Meyers, P.A., 1997. Organic geochemical proxies of paleoceanographic, paleolimnologic and paleoclimatic processes. Org. Geochem. 27, 213–250.
Miall, A.D., 1978. Facies types and vertical profile models in braided river deposits: a summary. In: Miall, A.D. (Ed.), Fluvial sedimentology. Canadian Society of Petroleum Geologists, Calgary, pp. 597–604.
Mildenhall, D.C., Brown, L.J., 1987. An early Holocene occurrence of the mangrove Avicennia marina in Poverty Bay, North Island, New Zealand: its climatic and geological implications. N. Z. J. Bot. 25, 281–294.
Miotto, J.A., 1993. Sismicidade e zonas sismogênicas do Brasil (Doctoral Thesis). Universidade Estadual Paulista, Rio Claro, Brazil.
Mörner, N.-A., 1996. Global change and interaction of earth rotation, ocean circulation and paleoclimate. An. Acad. Bras. Cienc. 68, 77–94.
Mörner, N.A., 1999. Sea-level and climate: rapid regressions at local warm phases. Quat. Int. 60, 75–82.
Moseley, M.E., Feldman, R.A., Ortloff, C.R., Narvaez, A., 1983. Principles of agrarian collapse in the Cordillera Negra, Peru. Ann. Carnegie Mus. 52, 299–327.
Nials, E.L., Deeds, E.E., Moseley, M.E., Pozorski, S.G., Pozorski, T.G., Feldman, R.A., 1979. El Niño: the catastrophic flooding of coastal Peru. Field Mus. Nat. Hist. Bull. 50, 4–14.
Pessenda, L.C.R., Boulet, R., Aravena, R., Rosolen, V., Gouveia, S.E.M., Ribeiro, A.S., Lamote, M., 2001. Origin and dynamics of soil organic matter and vegetation changes during the Holocene in a forest-savanna transition zone, Brazilian Amazon region. The Holocene 11, 250–254.
Pessenda, L.C.R., Ribeiro, A.S., Gouveia, S.E.M., Aravena, R., Boulet, R., Bendassolli, J.A., 2004. Vegetation dynamics during the late Pleistocene in the Barreirinhas region, Maranhão State, northeastern Brazil, based on carbon isotopes in soil organic matter. Quat. Res. 62, 183–193.
Peterson, L.C., Haug, G.H., 2006. Variability in the mean latitude of the Atlantic Intertropical Convergence Zone as recorded by riverine input of sediments to the Cariaco Basin (Venezuela). Palaeogeogr. Palaeoclimatol. Palaeoecol. 234, 97–113.
Posamentier, H.W., Allen, G.P., James, D.P., Tesson, M., 1992. Forced regressions in a sequence stratigraphic framework: concepts, examples, and exploration significance. Am. Assoc. Pet. Geol. Bull. 76, 1687–1709.
Poveda, G., Mesa, O.J., 1997. Feedbacks between hydrological processes in tropical South America and large-scale ocean-atmospheric phenomena. J. Clim. 10, 2690–2702.
Pugh, D.T., 1987. Tides, surges and mean sea-level: a Handbook for Engineers and Scientists. Wiley, London 486 pp.
Quinn, W.H., Neal, V.T., Antunez de Mayolo, S., 1987. El Niño occurrences over the past four and a half centuries. J. Geophys. Res. 92, 14,449–14,461.
Reimer, P.J., Baillie, M.G.L., Bard, E., Bayliss, A., Beck, J.W., Bertrand, C.J.H., Blackwell, P.G., Buck, C.E., Burr, G.S., Cutler, K.B., Damon, P.E., Edwards, R.L., Fairbanks, R.G., Friedrich, M., Guilderson, T.P., Hogg, A.G., Hughen, K.A., Kromer, B., McCormac, F.G., Manning, S.W., Ramsey, C.B., Reimer, R.W., Remmele, S., Southon, J.R., Stuiver, M., Talamo, S., Taylor, F.W., Van der Plicht, J., Weyhenmeyer, C.E., 2004. IntCal04 terrestrial radiocarbon age calibration, 26–0 ka BP. Radiocarbon 46, 1029–1058.
Roosevelt, A.C., 1991. Moundbuilder of the Amazon: geophysical archaeology on Marajó Island, Brazil. Academic Press, San Diego.
Rosario, R.P., Bezerra, M.O.M., Vinzon, S.B., 2009. Dynamics of the saline front in the Northern Channel of the Amazon River — influence of fluvial flow and tidal range (Brazil). J. Coast. Res. 2, 503–514.
Rossetti, D.F., Goés, A.G., Valeriano, M.M., Miranda, M.C.C., 2007. Quaternary tectonics in a passive margin: Marajó Island, northern Brazil. J. Quat. Sci. 22, 1–15.
Rossetti, D.F., Almeida, S., Amaral, D.D., Lima, C.M., Pessenda, L.C.R., 2010. Coexistence of forest and savanna in an Amazonian area from a geological perspective. J. Veg. Sci. 21, 120–132.
Rossetti, D.F., Souza, L.S.B., Prado, R., Elis, V.R., 2012. Neotectonics in the northern equatorial Brazilian margin. J. S. Am. Earth Sci. 37, 175–190.
Röthlisberger, F., Hass, P., Holzhauser, H., Keller, W., Bircher, W., Renner, F., 1980. Holocene climatic fluctuations—radiocarbon dating of fossil soils (fAh) and woods from moraines and glaciers in the Alps. Geogr. Helv. 35, 21–52.
Roubik, D.W., Moreno, J.E., 1991. Pollen and spores of Barro Colorado Island. Missouri Botanical Garden (268 pp.).
Rudddiman, W.F., 2008. Earth's climate — past and future. W.H. Freman and Company, New York (388 pp.).
Sandweiss, D., 1986. The beach ridges at Santa, Peru: El Niño, uplift, and prehistory. Geoarchaeology 1, 17–28.
Schidlowski, M., Hayes, J.M., Kaplan, I.R., 1983. Isotopic inferences of ancient biochemistries: carbon, sulphur, hydrogen and nitrogen. In: Scholf, J.W. (Ed.), Earth's Earliest Biosphere, Its Origin and Evolution. Princeton University Press, Princeton, pp. 149–186.
Scholl, D.W., 1964. Recent sedimentary record in mangrove swamps and rise in sea level over the southwestern coast of Florida: part 1. Mar. Geol. 1, 344–366.
Semeniuk, V., 1994. Predicting the effect of sea-level rise on mangroves in Northwestern Australia. J. Coast. Res. 10, 1050–1076.
Smith, C.B., Cohen, M.C.L., Pessenda, L.C.R., França, M.C., Guimarães, J.T.F., 2012. Holocenic proxies of sedimentary organic matter and the evolution of Lake Arari-Amazon Region. Catena 90, 26–38.
Snedaker, S.C., 1982. Mangrove species zonation: why? In: Sen, D.N., Rajpurohit, K.S. (Eds.), Contributions to the Ecology of HalophytesTasks for Vegetation Science vol. 2. W. Junk, The Hague, pp. 111–125
Solomina, O., Jomelli, V., Kaser, G., Ames, A., Berger, B., Pouyaud, B., 2007. Lichenometry in the Cordillera Blanca, Peru: "Little Ice Age" moraine chronology. Glob Planet. Chang. 59, 225–235.
Sommerfield, K.C., Nittrouer, C.A., Figueiredo, 1995. Stratigraphic evidence of changes in Amazon shelf sedimentation during the late Holocene. Mar. Geol. 125, 351–371.
Sommerfield, C.K., Nittrouer, C.A., Figueredo, A.G., 2004. Stratigraphic evidence of changes in Amazon shelf sedimentation during the late Holocene. Mar. Geol. 125, 351–371.
Souza, E.J., Pinheiro, R.V.L., 2009. Relações entre as estruturas tectônicas do embasamento e o desenvolvimento da paisagem da região costeira do estado do Amapá uma investigação sobre reativações tectônicas e acumulação de hidrocarbonetos. Relatório técnico-científico. ANP, Brasília (105 pp.).
Spear, F.S., 1993. Metamorphic Phase Equilibria and Pressure-Temperature-Time Paths. Mineralogical Society of America, Washington, D.C. 799p.
Taylor, S.R., McLennan, S.M., 1985. The continental crust: its composition and evolution. Geol. Mag. 122, 673–674.
Spenceley, A.P., 1982. Sedimentation patterns in a mangal on Magnetic Island near Townsville, North Queensland. Australia. Singap. J. Trop. Geogr. 3, 100–107.
Teixeira, J., 1630. Taboas gerães de toda a navegação. Library of the Congress, Washington, D.C. (http://hdl.loc.gov/loc.gmd/g3200m.gct00052. Cited 19 Mar 2013).
Thompson, L.G., Mosley-Thompson, E., Bolzan, J.F., Koci, B.R., 1985. A 1500 year record of tropical precipitation recorded in ice cores from the Quelccaya Ice Cap, Peru. Science 229, 971–973.
Thornton, S.F., McManus, J., 1994. Applications of organic carbon and nitrogen stable isotope and C/N ratios as source indicators of organic matter provenance in estuarine systems: evidence from the Tay Estuary, Scotland. Estuar. Coast. Shelf Sci. 38, 219–233.
Turekian, K.K., Wedepohl, K.H., 1961. Distribution of the elements in some major units of the earth's crust. Geol. Soc. Am. Bull. 72, 175.
Tyson, R.V., 1995. Sedimentary Organic Matter: Organic Facies and Palynofacies. Chapman and Hall, London 615pp.
Van der Hammen, T., 1974. The Pleistocene changes of vegetation and climate in tropical South America. J. Biogeogr. 1, 3–26.
Van der Hammen, T., 1986. Fluctuaciones holocenicas del nivel de inundaciones en la cuenca del Bajo Magdalena_Cauca-San Jorge (Colombia). Geol. Nor. 10, 11–18.
Vedel, V., Behling, H., Cohen, M.C.L., Lara, R.J., 2006. Holocene mangrove dynamics and sea-level changes in Taperebal, northeastern Pará State, northern Brazil. Vegetation History and Archaeobotany 15, 115–123.
Vilhena, M.P.S.P., Costa, M.L., Berrêdo, J.F., 2010. Continental and marine contributions to formation of mangrove sediments in an eastern Amazonian mudplain: the case of the Marapanim estuary. J. S. Am. Earth Sci. 29, 427–438.
Vinzon, B.S., Vilela, C.P.X., Pereira, L.C.C., 2008. Processos físicos na Plataforma Continental Amazônica. Relatório-Técnico, Potenciais Impactos Ambientais do Transporte de Petróleo e Derivados na Zona Costeira Amazônico. Petrobrás, Brasil (31 pp.).
Vital, H., Stattegger, K., 2000. Lowermost Amazon River: evidence of late Quaternary sea-level fluctuations in a complex hydrodynamic system. Quat. Int. 72, 53–60.
Walker, R.G., 1992. Facies, facies models and modern stratigrahic concepts. In: Walker, R.G., James, N.P. (Eds.), Facies Models — Response to Sea Level Change. Geological Association of Canada, Ontario, pp. 1–14.
Wedepohl, K.H., 1995. The composition of the continental crust. Geochim. Cosmochim. Acta 59, 1217–1232.
Wells, J.T., Coleman, J.M., 1978. Longshore transport of mud by waves: Northeastern coast of South America. Geol. Mijnb. 57, 353–359.
Wolanski, E., Mazda, Y., King, B., Gay, S., 1990. Dynamics, flushing and trapping in Hinchinbrook Channel, a giant mangrove swamp, Australia. Estuar. Coast. Shelf Sci. 31, 555–579.
Woodroffe, C.D., 1982. Geomorphology and development of mangrove swamps, Grand Cayman Island, West Indies. Bull. Mar. Sci. 32, 381–398.
Woodroffe, C.D., Mulrennan, M.E., Chappell, J., 1993. Estuarine infill and coastal progradation, southern van Diemen Gulf, northern Australia. Sediment. Geol. 83, 257–275.
Zhang, R., Delworth, T.L., 2005. Simulated tropical response to a substantial weakening of the Atlantic thermohaline circulation. J. Clim. 18, 1853–1860.